

Semi-supervised Image Attribute Editing using Generative Adversarial Networks*

Yahya Dogan

Ankara University

Computer Engineering Department

yahyadogan@ankara.edu.tr

Hacer Yalim Keles

Ankara University

Computer Engineering Department

hkeles@ankara.edu.tr

Abstract

Image attribute editing is a challenging problem that has been recently studied by many researchers using generative networks. The challenge is in the manipulation of selected attributes of images while preserving the other details. The method to achieve this goal is to find an accurate latent vector representation of an image and a direction corresponding to the attribute. Almost all the works in the literature use labeled datasets in a supervised setting for this purpose. In this study, we introduce an architecture called Cyclic Reverse Generator (CRG), which allows learning the inverse function of the generator accurately via an encoder in an unsupervised setting by utilizing cyclic cost minimization. Attribute editing is then performed using the CRG models for finding desired attribute representations in the latent space. In this work, we use two arbitrary reference images, with and without desired attributes, to compute an attribute direction for editing. We show that the proposed approach performs better in terms of image reconstruction compared to the existing end-to-end generative models both quantitatively and qualitatively. We demonstrate state-of-the-art results on both real images and generated images in MNIST and CelebA datasets.

Keywords — Image attribute editing, generative models, generative adversarial networks, Deep learning, convolutional neural networks

1 Introduction

The aim of generative models is to produce synthetic images, which are similar to samples in a dataset. Recently, remarkable approaches have been proposed and developed in this field [1–4]. Each of these approaches has their own strengths and weaknesses. Generative Adversarial Networks (GANs) [1] dominate this field in terms of generating sharp images and having a meaningful latent representation with a rich linear structure [5,6]. GANs are composed of two networks, i.e. generator and discriminator, that compete with each other during training for learning the underlying distributions of the images. Given a latent vector z , which is randomly drawn from normal or uniform distribution, namely $P(Z)$, the generator produces a synthetic image. The discriminator, on the other hand, determines whether a given image is real or fake. The discriminator produces a probability/score value that shows the probability/score of the given image as being a real image. Depending on the objective function that maximizes the discrimination of real and fake images, parameters of both networks, i.e. generator and discriminator, are optimized. It's only after the Nash equilibrium that is established between the two networks, the discriminator hardly differentiates given images as real or fake with confidence. This state is a good indicator for the generator model that the generated images are similar to the real data distribution. After the training is completed, the discriminator is discarded and the generator is used for mapping from the latent space to the image space.

Although a GAN generator provides a means for generation of different images using random latent vectors, it is difficult to model the inverse function for the generator model so that images can be

*Note that this paper is under consideration at Neurocomputing Journal.

manipulated in a controlled setting; especially for high resolution image generators. Existing methods apply algebraic operations in the latent vector space to encode semantically meaningful attributes to images. In DCGAN work [5], algebraic operations have been performed on latent vectors of two generated images with and without an attribute, such as a face containing sunglasses or not; the latent vector representing the attribute is added to the latent vector corresponding to a generated image to provide the image with the attribute. However, due to use of randomly generated images, such vector additions manipulate other attributes as well as the desired attribute; hence usually cause significant changes in the original face attributes. The challenge here is to find a latent vector representation and a proper direction that corresponds to the factors that changes only the desired attribute; the produced images will be the same with the original source and they are different only for the encoded attribute. This operation requires accurate mapping from the image space to the latent space and identification of the true latent direction. In this work, we propose a novel architecture for solving both problems accurately. The proposed architecture is composed of an encoder and generator networks. The training of the networks are performed in an unsupervised setting, i.e. no attribute labels are used. Semi-supervision is performed in the calculation of desired attribute directions using the encoder network. We show that the proposed solution is effective for controlled manipulation of images.

The main contributions of this work can be summarized as follows:

(1) We propose a new straightforward end-to-end architecture called Cyclic Reverse Generator (CRG) that allows learning the inverse of the generator in an unsupervised setting and allows reconstruction of both generated and real images in high quality.

(2) We obtain a latent vector direction for attribute editing using our CRG encoder using only an arbitrary pair of real images; one with and the other without an attribute.

(3) Keeping the other attributes the same, we show that it is possible to manipulate only the desired attributes at any rate.

(4) We give state-of-the-art results on CelebA dataset [7] to reconstruct an image at 128x128 resolution, which is the highest resolution that is obtained using an architecture with an encoder that is connected end-to-end to a generator.

The rest of the paper is organized as follows. A brief summary of the related previous works are summarized in Section 2. The proposed method is discussed in detail in Section 3. The results of our image reconstructions are provided in Section 4. The paper is concluded with future directions.

2 Related Works

In GANs, the studies of manipulating desired attribute(s) of images can be divided into two main groups, as semi-supervised and unsupervised methods. In the first group, training is performed using a code representing each attribute in a conditional GAN architecture [8–11]. In these methods, after training, selected attributes of given images can be changed. However, the requirement of labeled datasets makes these methods impractical. Moreover, the attributes are limited with the trained labels. In the second group, i.e. unsupervised methods, the main purpose is to construct a model that learns the hidden structures in image generation and to inverse the generation process without using attribute labels. Our work belongs to this group. The studies in this group can be examined under three categories: The first one is Gradient Based Techniques (GBTs) [12, 13]. In these approaches, latent vector corresponding to an image is taken as the optimization goal; the aim is to find latent vector z' corresponding to $\phi(z)$ image. These methods do not require an additional encoder network. A pre-trained generator network is used to perform this process. Firstly, a z' vector is sampled randomly from a prior distribution and it is given to the generator. According to the gradient obtained from the difference between the generated image and the target image, the z' vector is updated. After numerous iterations, the z' vector is expected to converge to the target vector z that represents the $\phi(z)$ image. In GBTs, the encoding of the latent vector representation is obtained after a great number

of gradient descent steps, which makes these approaches impractical. The structure of the GBT and the optimization function is depicted in Fig. 1.

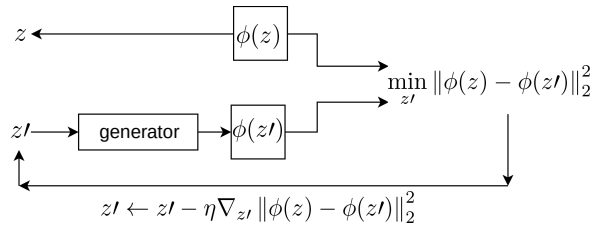


Fig. 1: The structure of the GBT [12].

The second category includes architectures with an encoder network, in addition to the generator and the discriminator networks [14–17]. These studies differ depending on how the encoder network is used and trained in the architecture. In the VAEGAN [14], the generator is constructed using the decoder of a variational autoencoder (VAE), and encoder-decoder-discriminator networks are combined end-to-end as a single network. This structure enables reconstruction of more realistic and sharper images compared to VAEs. Unlike the VAEGAN, in BiGAN [15] and ALI [16] studies, neither generator nor encoder can see each other’s outputs; in both works, the discriminator is trained to distinguish tuples of samples with their latent codes. In studies belonging to the second category, generally three networks are trained simultaneously. This makes it difficult to train encoder using a pre-trained generator. Another disadvantage of studies in this category is that they are inadequate to generate high-resolution synthetic images; most of these studies cannot go beyond 64x64 resolutions [18]. Moreover, most of these studies fail to extract the latent vector representation of an image that changes only a subset of attributes while preserving the other properties as they are. Another study in this category is the AEGAN architecture [17]. The difference of this architecture from the others is that the encoder network is not trained simultaneously with the other networks. In this study, encoder-generator architecture is created by using a pre-trained generator model and an encoder network is trained from scratch. The encoder network is not trained with real images but is trained only with the generated images. The results of the reconstructions of the generated images are better than the real images; yet they are both not very successful.

The third category is Adversarial Generator-Encoder (AGE) architectures whose structure does not contain a discriminator network and an adversarial game is set up directly between the encoder and the generator [18, 19]. In this category, training is performed using a combination of adversarial loss and reconstruction loss that encourages the encoder and generator to be reciprocal. There are three main advantages of these architectures: (1) Since adversarial loss is calculated between encoder and generator, there is no need for a discriminator and the number of learned parameters decreases, (2) In GANs, distributions are usually compared in high dimensional image space, in AGE, comparison is performed in a simpler latent space, (3) The encoder network is given both real and fake images as input, so the real images are better encoded. When outputs of this architecture are examined, it is seen that it produces better results than other end-to-end architectures for 64x64 resolutions, but it cannot go beyond 128x128 resolutions for reconstruction of images and the results at this resolution are not at desired level. Considering the studies in this category, it is seen that they are poor in terms of image quality and diversity compared to the models with a discriminator [20]. Furthermore, if reconstruction loss is not used in AGE architecture, encoder and generator mapping is not reciprocal. In order to make networks reciprocal, reconstruction loss is controlled by a hyper-parameter in the objective function. However, the determination of the value of this parameter brings extra burden. To overcome the problems mentioned in this category, in this work we propose an architecture with two separate parts that have cyclic connections with each other and perform training in two steps. In the first step, a generator is trained using the original adversarial loss between the generator and discriminator [20]. In the second step, the encoder network is trained from scratch by using the cyclic connection between the encoder and the generator. This architecture allows generator network to receive a latent vector, which is either randomly generated or encoded, as an input, and the encoder network to get either real

or fake images as input during training. This approach helps convergence problems of encoders during training. Moreover, it has an additional benefit that it enables learning the inverse mapping of any pre-trained generator that are readily available for generation of images in different domains.

The success of the encoder network is directly related to the success of the generator in mapping latent vectors to images. Two main problems arise in generator training, especially when high-resolution images are used. The first problem is the stability problem; competition between the two networks, i.e. generator and discriminator, creates instability, since one dominates the other. The second problem is the mode collapse problem; the generator network produces samples in limited varieties. Recently, new objective functions [21–25], regularization techniques [22, 26] and network architectures [5, 20, 25] have been proposed to overcome the stability problem. In order to prevent mode collapse problem, generating similar images are prevented using similarities of the samples in the discriminator networks [20, 27]. Although there is various GAN research that generate high quality images for popular datasets, it is not clear which algorithm is superior to the others. In a recent study, the state-of-the-art models have been compared objectively using some well-known evaluation metrics [28]. In this study, it is reported that the performance of the models largely depends on datasets and hyper-parameter optimization; there is no ideal model that consistently generate high quality images in all datasets. Therefore, it is a challenge to determine the appropriate architecture, objective function and regularization techniques for different datasets.

In addition to the vast literature about GAN training, there are recent works that focus on generating images with different attributes by encoding those attributes as part of the latent code. It is still a challenging problem, since the encoding of the desired attributes in the latent space is entangled. Therefore, it is difficult to change only a subset of attributes without changing other properties of the image. In the StyleGAN [29], research has been carried out on making the latent vector disentangled by using the generator structure used in the style transfer literature [30]. The aim is to find a latent vector that is composed of linear subspaces, such that each subspace controls an attribute. With this architecture, low, medium and high level attributes in the image can be modified by changing the determined subspaces of the latent space corresponding to the image. Still yet, the changes in this subspace changes other attributes of the image as well as the desired attributes.

3 The Method

3.1 The Cyclic Reverse Generator (CRG) Model

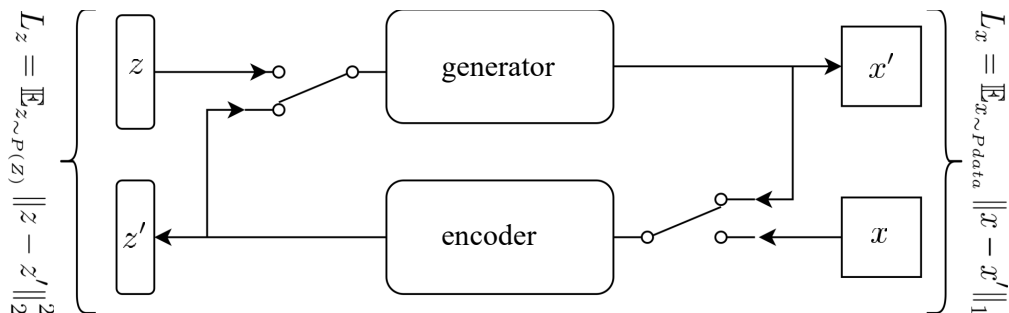


Fig. 2: CRG architecture

This section introduces the proposed model for the reconstruction of an image. Our model is composed of two parametric networks: the generator network $g_\omega(z)$ that maps the latent space z to the data space x , and the encoder network $e_\epsilon(z)$ that maps the image x from the data space to the latent space z . The goal is to ensure that the encoder and the generator networks have bidirectional connections for generating and encoding of either real or fake images. The design of the proposed model is shown in Fig. 2. The reconstruction loss is calculated using the error in the image space and the error in the latent space together, in an order, during encoder training.

We first train the GAN architecture, i.e. generator and discriminator networks, until we obtain state-of-the-art scores for the selected datasets. We observed that, it is only after an optimum generator is trained that a successful mapping can be done from the image space, x , to the latent space, z . Our first expectation from the model is the ability to reconstruct the latent representation of randomly generated samples. For a given random z , the generator generates an image; giving that image to the encoder network an estimated z is obtained. We minimize the objective in (1) to minimize the error between the estimated, i.e. $e_\epsilon(g_\omega(z))$, and the initial z .

$$\hat{\epsilon} = \underset{\epsilon}{\operatorname{argmin}}(\mathbb{E}_{z \sim P(Z)} \|z - e_\epsilon(g_\omega(z))\|_2^2) \quad (1)$$

Our second expectation from the model is the ability to reconstruct real images. This is also important because we want to be able to compute the relevant directions related to an attribute in the latent z space using sample real images. For a given image x , the encoded z value is used to reconstruct the image, i.e. $g_\omega(e_\epsilon(x))$, we use the objective in (2) to minimize the error between the reconstructed image and the original image.

$$[!h]\hat{\epsilon} = \underset{\epsilon}{\operatorname{argmin}}(\mathbb{E}_{x \sim P_{data}} \|x - g_\omega(e_\epsilon(x))\|_1) \quad (2)$$

In each iteration, the parameters of the encoder are updated twice, using the objective in (1) and (2), respectively.

We call our proposed architecture as Cyclic Reverse Generator (CRG) (Fig. 2), since the encoder learns the inverse function of the generator using the proposed cyclic error minimization. In the model, the encoder is given either real or generated images, and the generator is given either a randomly generated or an encoded latent vector as the input. This enables both generated and real images to be reconstructed. We use a pre-trained generator in the CRG architecture. In this setting, only the encoder parameters are updated. Generally, end-to-end approaches implement simultaneous training of three networks. In this case, the dominance of one of the networks in the architecture usually leads to instability problems. Therefore, a pre-trained generator is not used in these studies. However, in CRG, the encoder is trained utilizing a pre-trained generator without facing stability problems. This is advantageous since we can train an encoder for a GAN model that is already trained for different domains.

3.2 Training The Models

In this section, we provide the training details for the GAN and the CRG architecture using the two well-known and widely used datasets in this domain, i.e. MNIST and CelebA datasets.

Recently, a lot of researchers are working actively in the GAN domain and it is a challenge to determine which architecture(s) and objective function(s) are better suited for training a GAN for a particular dataset. Authors of [28] argue that the performance of recently proposed state of the art models heavily depends on datasets, and that no particular model is strictly dominating the others. This study has been our reference for the selection of the objective functions for the MNIST and the CelebA datasets in this research; we use the Non-Saturating GAN (NSGAN) for the MNIST dataset and WGAN-GP for the CelebA dataset in this work.

3.2.1 MNIST Model

The MNIST dataset [31] contains handwritten images of digits in 28x28 pixel resolution. It contains 60000 grayscale images for training and 10000 grayscale images for testing. We use the DCGAN architecture, which has a simple structure, yet produce successful images without stability or mode collapse problems. Although WGAN [21] produces the best scores for the MNIST dataset, we use NSGAN

objective function since it does not have weight clipping hyper-parameter as in WGAN, which requires additional adjustment. Table 1 shows the details of the generator and the discriminator architecture that we use in this dataset. The generator consists of a fully connected layer, two deconvolution layers and a convolution layer. The tanh activation function is used in the last layer of the generator, and leaky ReLU activation [32] is used in the other layers with a slope value of 0.2. The generator is given a 100-dimensional latent vector drawn from a uniform distribution, in the range $[-1, 1]$, as the input. On the other hand, the discriminator consists of two convolutional layers and a fully connected layer. The sigmoid activation function is used in the last layer of the discriminator, and leaky ReLU is used after the convolutions. We train the generator and the discriminator using Adam optimizer [33] with a batch size of 256, setting the learning rate to $2e - 4$ and *beta_1* to 0.5.

Table 1: Architectural details of the three networks that we used for the MNIST dataset.

Generator network					
Input Shape: 100					
Operation	Kernel	Stride	Filter	Activation	Dropout
Dense	-	-	128*7*7	LReLU	-
Reshape	-	-	(7x7)*128	-	-
Deconv2D	5x5	2	128	LReLU	-
Deconv2D	5x5	2	64	LReLU	-
Conv2D	5x5	1	1	LReLU	-
Discriminator network					
Input Shape: 28x28x1					
Conv2D	5x5	2	64	LReLU	0.3
Conv2D	5x5	2	128	LReLU	0.3
Flatten	-	-	7x7x128	-	-
Dense	-	-	1	Sigmoid	-
Encoder network					
Input Shape: 28x28x1					
Conv2D	5x5	2	32	LReLU	0.3
Conv2D	3x3	1	64	LReLU	0.3
Conv2D	5x5	2	128	LReLU	0.3
Conv2D	3x3	1	256	LReLU	0.3
Conv2D	3x3	1	512	LReLU	0.3
Flatten	-	-	7x7x512	-	-
Dense	-	-	100	Tanh	-

We train the generator and the discriminator for 250 epochs. In the first few iterations of training, the discriminator can distinguish real and generated images with high confidence. However, as the training progress, the images generated by the generator converge to the real samples drawn from the data distribution. At that point, it becomes difficult for the discriminator to distinguish the real and fake images. After the GAN training, the discriminator is discarded and the generator is used in the proposed the CRG architecture (Fig. 2), for training the encoder.

The encoder architecture is structurally similar to the discriminator. There are a few differences between these two networks: (1) since the output of the encoder will be used as an input for the generator, the output layer of the encoder contains 100 neurons, (2) tanh activation function was used in the last layer to obtain a distribution in $(-1, 1)$ range, and (3) after each convolution layer, batch normalization [34] is used to transfer the gradients to the earlier layers. In order to avoid overfitting, we also use 30% dropout [35] in both the discriminator and the encoder networks. Pooling layer is not used in any of the networks, instead, in some layers of the encoder, we set the stride parameter as 2 to reduce the size of the image. In the layers with a stride value of 2, the filter size is configured as 5x5 and in the others, i.e. with a stride of 1, the filter sizes are set as 3x3. In the CRG architecture training, we use Adam optimizer, which has the same parameters as the one we used to train the GAN model, for 200 epochs.

3.2.2 CelebA Model

The CelebA dataset contains 202599 celebrity images with large pose variations, taken from different backgrounds. In this study, we use 30000 images in 128x128 pixel resolution. Most of the models that infer the latent z vectors work with 32x32 resolution images. There are very few models that go beyond 64x64 pixel resolution [18]. Current state-of-the-art models in the z inference produce a maximum of 128x128 images. However, the quality of the images is not sufficiently good for the reconstruction of the real images that are necessary to find the latent vector corresponding to an attribute. The reason for this is that as image resolution increases, stability and diversity problems become more apparent in GAN training. Hence, in order to achieve the purpose of this research, we need to train a generator that enable us to generate high-resolution images without encountering stability and diversity problems.

The Generator Network: There are some design choices to be made when training a generator network to generate high-resolution images; selection of the objective function, used regularization technique, selected GAN architecture and selection of the hyper-parameter values. For the CelebA dataset, we use the same model that we proposed in our preliminary work [36]. The model is similar to the Progressive GAN (PGGAN) architecture. In GAN studies, as the image resolution increases, the discriminator distinguishes between real and generated images easily. This causes imbalance problem between the two networks during training. The key idea in PGGAN is to grow both the generator and the discriminator progressively to capture fine details in images. Initially, the training of both networks is started with a low spatial resolution, i.e. 4x4 pixel images, and as the training progresses, a new layer is added to both networks to increase the spatial resolution of the generated images. In addition, to ensure the stability between the two networks, we apply spectral normalization [26] to both the generator and the discriminator as in SAGAN [37], we keep the learning rates of the discriminator more than the generator as in TTUR [38], i.e. we use $1e - 4$ and $2e - 4$ learning rate for the generator and the discriminator, respectively. We optimize the generator and the discriminator by 1:2 rate.

Table 2: Performance comparison of the generator networks for 128x128 pixel resolution.

	FID [38]	Latent vector dimension
AGE [19]	154.79	512
Pioneer [18]	23.15	512
Our Model	9.4	128

In Table 2, we compare our generator with the AGE and Pioneer [18] generators for 128x128 pixel resolution, since these models contain a model that infer the latent z vectors similar to ours. Pioneer is the progressive model of the AGE architecture. We use the Fréchet Inception Distance (FID) metric, which is a commonly used metric to compare generator networks in terms of image quality and diversity. A low FID score indicates a better generator. Note that our generator produces a lower FID score, even though it has a 128 dimensional latent space, instead of 512. The results also depict that using a model with a discriminator produces better scores. In Fig. 3, we show the interpolation capability between randomly generated images using our generator. The quality of the generated images is apparent in these randomly generated samples.

The Encoder Network Architecture: The generator described in the previous section contains approximately 22 million trainable parameters. In general, we observe that keeping the capacity of the encoder higher than the generator provides better encoding. The encoder consists of 6 blocks with a total of approximately 26 million trainable parameters. Training deep CNNs from scratch can cause convergence problems during the network training and training time increases substantially [39]. Given the fact that CNNs encode low-level features in the first few layers, we use the first 4 blocks of the pre-trained VGG-16 Net [40] in the encoder architecture with a list of modifications: (1) we remove



Fig. 3: Sample interpolations of our generator between two generated images.

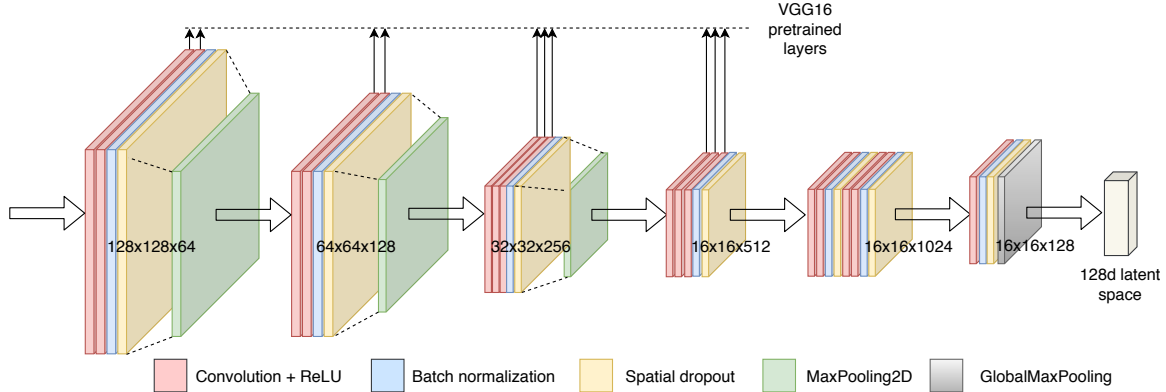


Fig. 4: The Encoder network architecture.

the fourth max-pooling layer, so as not to reduce image resolution too much, (2) we include a batch normalization layer at the end of each convolution block to overcome the vanishing gradient problem that occurs when we include additional blocks at the end, (3) to avoid overfitting, we use spatial dropout layer after the batch normalization layers. In order to increase the capacity of the network, we include two new blocks to extract features that are specific to CelebA dataset. Finally, we use global max pooling on the last layer of the encoder. There are 64 filters in the first block and the number of filters in the consecutive blocks are doubled except for the last block; since the latent vector dimension is 128, we use 128 filters in the last block. We use a 3x3 filter size in the convolution layers, except for the 1x1 transposed convolution layer in the last convolution layer. The structure of the encoder is depicted in Fig. 4.

Training details: We trained the encoder using the CRG architecture as we explained in Section 3.1. As previously mentioned in the CRG, MAE loss is used in the image space and MSE loss is used in the latent space, and only the parameters of the encoder are optimized at each iteration. During the training, all of the weights of the convolutional layers of the encoder, including the pretrained weights of the VGG Network, are trained using the same learning rate. We train the encoder using RMSProp optimizer [41] with a batch size of 128, setting rho to 0.9 and epsilon to $1e - 08$. In order to adapt the existing VGG layer weight values properly, we use a small learning rate, i.e. $1e - 4$, for optimizing all the parameters in the encoder architecture. We reduce the learning rate by a factor of 2 when minimum validation loss stops improving for 10 epochs. To avoid overfitting, we apply different regularizations in the training; we use 50% spatial dropout, and data augmentation where we rotate the images in the range of 30 degrees and apply horizontal and vertical flips. Model checkpoint is used to save the best model and using early stopping, we end the training process if no improvement is achieved in the validation loss for 20 epochs. After the training process, we expect that the generated images and their reconstructions look almost the same, and that the reconstructions of the real images are at an acceptable level; sufficient to find accurate latent vector directions for the attribute embedding.

3.3 Computing Latent Attribute Representations

In the CRG architecture, the encoder is trained completely without any supervision; we do not use any labels or encode conditions during GAN training (please refer to Section 3.2 for details). In order to extract the latent vector corresponding to an attribute, we use an arbitrary real image as a reference and a second image that contains a particular attribute that we want to control. In Fig. 5, we demonstrate the extraction of the latent vector direction for smile attribute embedding. We first use our encoder to get the latent vectors of the reference images. Then compute the normalized direction in the latent space to determine the relevant attribute direction.

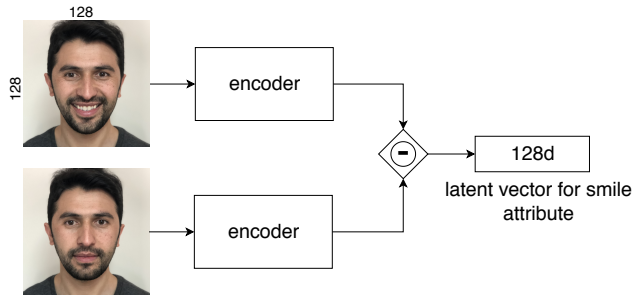


Fig. 5: Extraction of the latent vector corresponding to smile attribute.

When the accuracy of the generator and its inverse function, i.e. the encoder, is high, this direction accurately changes only the relevant attribute by preserving the other attributes in the image. Equation (3) is used to find the latent vector direction representing an attribute f .

$$z_f = \frac{z_1 - z_2}{\|z_1 - z_2\|_2^2} \quad (3)$$

Where z_1 is the latent code that is generated by the encoder using a reference image and z_2 is the latent code obtained using an image that has the desired attribute. After z_f is obtained, equation (4) is used to generate an image with the desired attribute.

$$z_a = z_p + k * z_f \quad (4)$$

Where z_p is the latent vector estimated by the encoder using any arbitrary image, k is the amount of attribute that we want to impose into the image, z_a is the latent code of the attribute encoded image. The attribute encoding can be performed in positive or negative directions, as desired, by changing the sign of k accordingly in (4). To the best of our knowledge, the existing reconstruction models using GANs are not yet capable of accurately controlling only selected attributes in images. Modifying an image this way has three main advantages: (1) there is no need to have a labeled dataset to encode attributes, (2) attribute set is not constant; it can be constructed anyhow as long as a pair of arbitrary reference images are provided, (3) the amount of attribute injection to the target image can be controlled easily by adjusting one parameter, i.e. k .

4 Results and Discussion

This section provides comparisons of our CRG architecture with the related models designed for the concerned datasets and the results we obtained for image attribute editing at 128x128 pixel resolution using the CelebA dataset.

4.1 MNIST Model Experiments

In this section, we compare our CRG MNIST model with the BiGAN and Latent Regressor (LR) [15] models in terms of the reconstruction of the real images. We particularly chose BiGAN for comparison because it includes an optimized model for MNIST dataset. GANs are highly dependent on hyper-parameter settings and are optimized after an extensive search of the hyper-parameters for each dataset. We also compare our CRG model with the LR model. LR encoder is trained using only the generated images; hence the results also depict the performance of the LR encoder with real image inputs. In Fig. 6, we provide sample random real image reconstructions using BiGAN, LR and CRG models. Note that the appearance of the reconstructed images in the CRG model is better than the BiGAN and LR models. The produced images using the CRG architecture are almost identical to the real images.

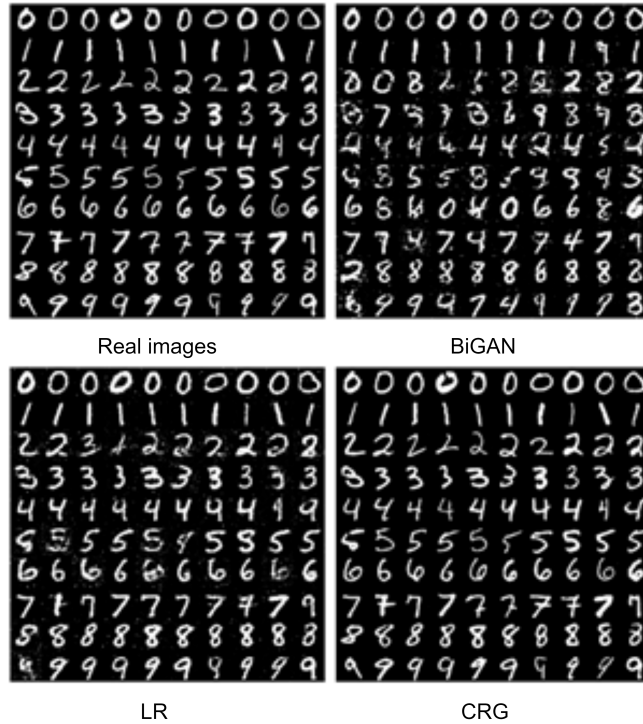


Fig. 6: Model outputs for the reconstruction of the real images.

The quantitative comparisons of the models are provided in Table 3, using mean squared error (MSE) and mean absolute error (MAE) for the test data (i.e. 10000 images). The proposed CRG architecture produce better results in terms of both metrics.

Table 3: Comparison of models with MSE and MAE metrics.

	MAE	MSE
BiGAN [15]	0.268	0.187
LR [15]	0.119	0.118
CRG	0.006	0.021

We also computed the difference hash (dhash) [42], perceptual hash (phash) [42] and wavelet hash (whash) [43] metrics to measure the similarity between the real and the reconstructed images. In these methods, images are initially converted into a fixed hash code. Then, the similarity between the original image hash code and the regenerated image hash code determines how the two images are similar. In Equation (5), HS represents hash similarity, BC represents hash bit count, i.e. 64 in our case, HD represents Hamming Distance between two BC hash codes. In Table 4, the results that are obtained for BiGAN, LR and our architecture using the MNIST test set are shown. As seen in Table 4, the CRG architecture has the highest similarity values in all the similarity measures.

$$HS_{O,R} = \frac{BC - HD(O,R)}{BC} \quad (5)$$

Table 4: The similarities of real images and reconstructed images.

	dhash	phash	whash
BiGAN [15]	0.749	0.766	0.832
LR [15]	0.823	0.866	0.838
CRG	0.979	0.977	0.964

4.2 CELEBA Model Experiments

In the Pioneer model [18], reconstruction of real images for 64x64 pixel resolution is compared with ALI and AGE studies, and the Pioneer model has been shown to be more successful than the others. Hence, we compare our CRG CelebA model with the Pioneer model. The other reason that we compare with only the Pioneer model is that other end-to-end studies do not have models that are optimized for 128x128 pixel resolution. In Fig. 7, we compare the two models in terms of the reconstruction performances using real images as input. Note that, although the generated images of both models are not exactly the same with the real input images, the reconstructed images using our CRG model look more similar to the input images; significant attributes of the input images are reflected to the generated images. Moreover, we noticed that the reconstructed images using the Pioneer model tend to be more blurry.



Fig. 7: Comparison of the Pioneer [18] and our CRG model for the reconstruction of real images. The images on the top row are used in the reconstruction.

We also quantitatively compare the models in Table 5, utilizing the image similarity metric that we used in MNIST dataset. The metrics also validate our visual judgments in Fig. 7 that the CRG model reconstructions are better than the Pioneer model reconstructions for real images.

Table 5: The similarities of real images and reconstructed images.

	dhash	phash	whash
Pioneer [18]	0.852	0.804	0.864
CRG	0.871	0.848	0.892

In order to change any attribute of a generated image, it is necessary to correctly reconstruct a generated image. In Fig. 8, we show the reconstruction of generated images using the Pioneer model. Fig. 9 shows the reconstruction of some generated images using our model. As can be seen from the samples, the encoder successfully learns the inverse mapping of the generator. When the two models



Fig. 8: Top row: Randomly generated images, bottom row: reconstructed images using the Pioneer model [18].

are compared, we also see that our model is more successful in the reconstruction of the generated images.



Fig. 9: Top row: Randomly generated images, bottom row: reconstructed images using our model.

4.3 Image Attribute Editing Experiments

In this section, we modify two arbitrary attributes, the smile and the pose adjustment attributes, to demonstrate the attribute encoding of a source image. We show the results of manipulating the smile attribute in two directions in Fig. 10 and the pose adjustment of the source images with neutral and smiling gestures in Fig. 11. As it is seen in the figures, with the exception of the interested attribute, other attributes of the source images are preserved substantially. These results are very promising for generating various synthetic images with desired attributes, which can be utilized in data augmentation for various problem domains. Using the proposed CRG training procedure, desired attributes can be injected to a source image without using a labeled dataset or conditional GANs architecture.

We also made experiments on changing more than one attribute simultaneously, on purpose, while preserving the source images. In Fig. 12, we show manipulation of the pose adjustment and the smile attributes simultaneously. The results exemplify multiple attribute editing using again only one pair of reference images.

Although our aim is to modify only a subset of attributes of the generated images, we also tested the model’s performance on real images. As shown in Fig. 13, we found that the results in the real images are also promising. We believe that the difference between the original source and the reconstruction is mainly due to using insufficient number of samples during our GAN training, i.e. 30000 real images. Generator may not know producing some novel attributes that it did not see before. For example, the earrings of the second sample in Fig. 13 is not produced since the generator has not seen enough samples with large earrings during training. However, the hair styles, gesture characteristics and the pose of the input images are successfully captured in the reconstructed images. The accuracy of real image reconstruction can be increased by using more samples with many attribute variations during GAN training.

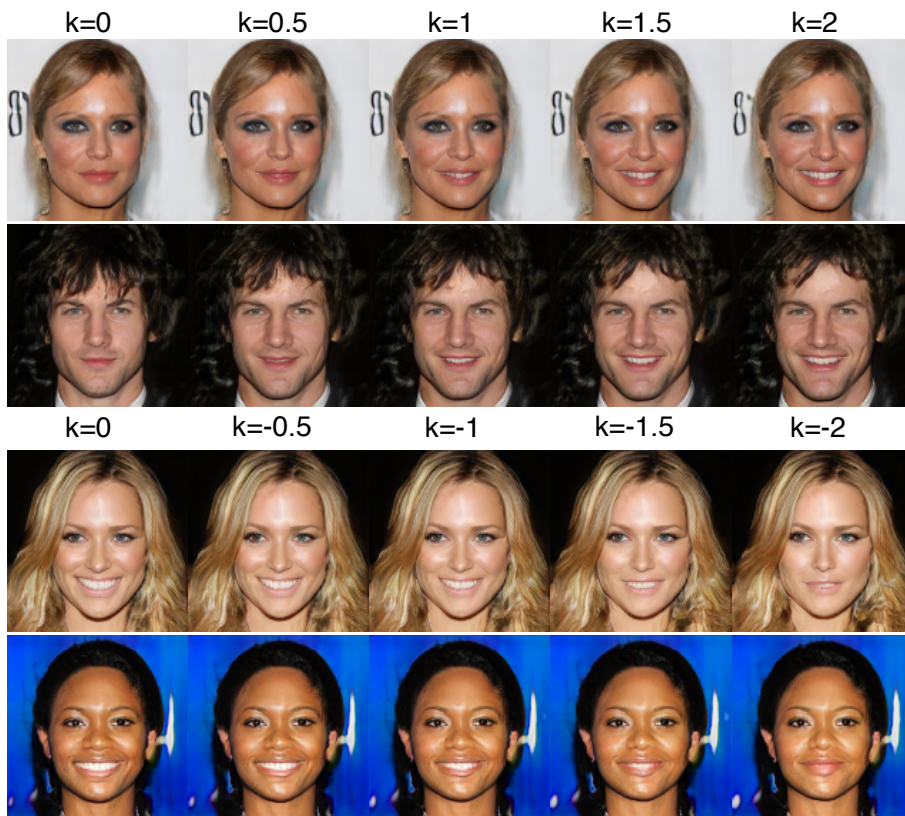


Fig. 10: Reducing or increasing the smile attribute in the generated images.

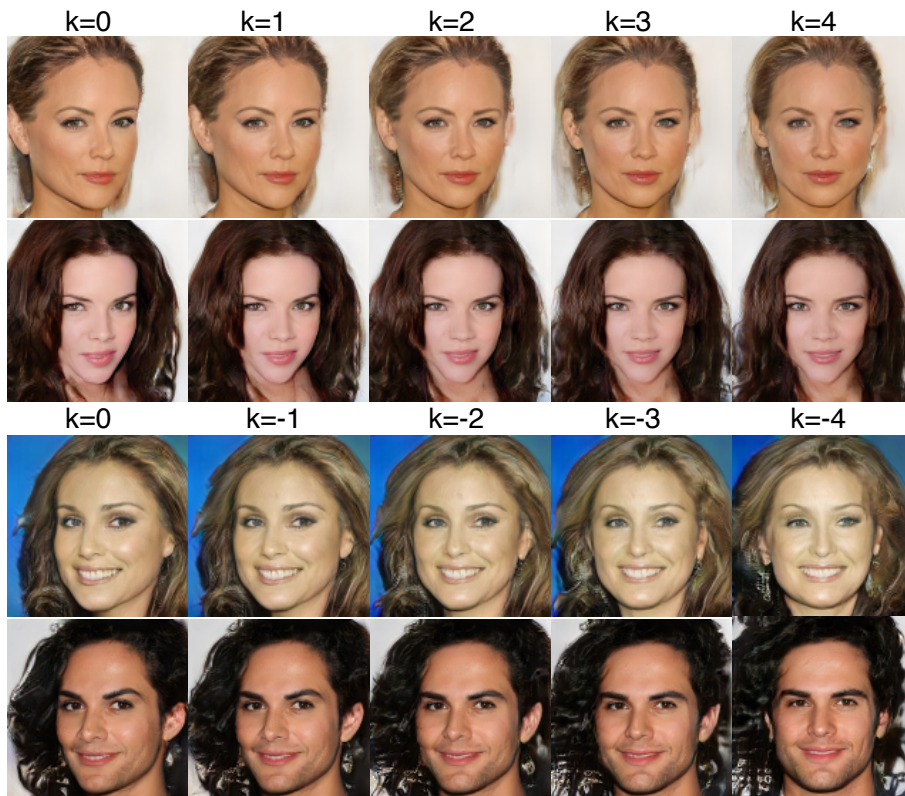


Fig. 11: Pose adjustment in the generated images.



Fig. 12: Modification of smile and head pose attributes.

Real Images

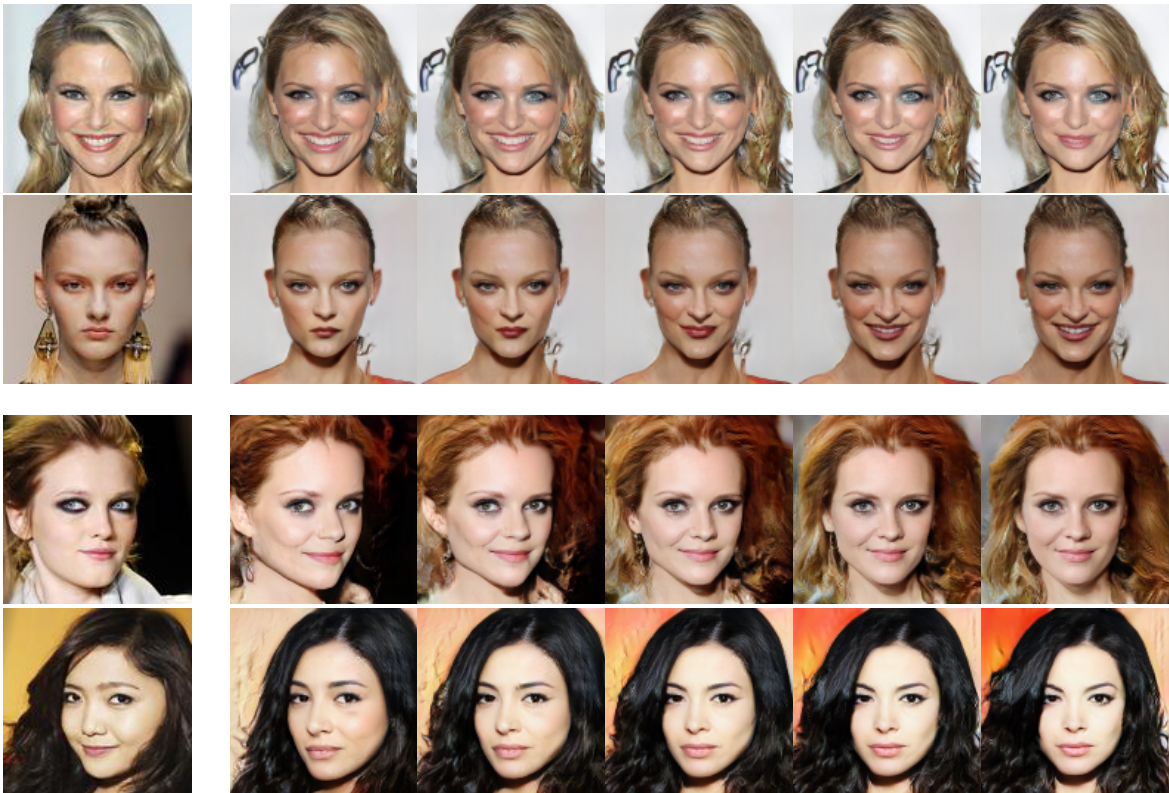


Fig. 13: Smile attribute and pose adjustment on real images.

5 Conclusion and Future Works

We introduced a novel CRG architecture that is effective learning the inverse of a given generator using cyclic error minimization without supervision. The proposed architecture can be used to compute the accurate latent representations of generated images for attribute editing. The attribute editing can be performed by providing a pair of real images that contains a source image with and without desired attributes. The results of the experiments show that the quality of the encoding is more successful than the state-of-the-art models. The rate of manipulation of the input images can be controlled dynamically using only one parameter. The set of attributes for editing is also dynamic and determined via reference images. Although the reconstruction of the generated images is very successful, the reconstruction performance of the model with the real images may be improved by using more training data with increased attribute variation. As a future work, in addition to increasing training data variation, we are also planning to train the encoder progressively, in parallel with generator training, to increase the reconstruction performance of the real images.

Acknowledgements

This research is funded by Ankara University (Scientific Research Projects Grant, grant id: 18L0443010).

References

- [1] I. Goodfellow, J. Pouget-Abadie, M. Mirza, B. Xu, D. Warde-Farley, S. Ozair, A. Courville, and Y. Bengio, “Generative adversarial nets,” in *Advances in neural information processing systems*, pp. 2672–2680, 2014.
- [2] D. P. Kingma and P. Dhariwal, “Glow: Generative flow with invertible 1x1 convolutions,” in *Advances in Neural Information Processing Systems*, pp. 10215–10224, 2018.
- [3] D. P. Kingma, T. Salimans, R. Jozefowicz, X. Chen, I. Sutskever, and M. Welling, “Improved variational inference with inverse autoregressive flow,” in *Advances in neural information processing systems*, pp. 4743–4751, 2016.
- [4] A. v. d. Oord, N. Kalchbrenner, and K. Kavukcuoglu, “Pixel recurrent neural networks,” *arXiv preprint arXiv:1601.06759*, 2016.
- [5] A. Radford, L. Metz, and S. Chintala, “Unsupervised representation learning with deep convolutional generative adversarial networks,” *arXiv preprint arXiv:1511.06434*, 2015.
- [6] M. Rosca, B. Lakshminarayanan, D. Warde-Farley, and S. Mohamed, “Variational approaches for auto-encoding generative adversarial networks,” *arXiv preprint arXiv:1706.04987*, 2017.
- [7] Z. Liu, P. Luo, X. Wang, and X. Tang, “Deep learning face attributes in the wild,” in *Proceedings of the IEEE international conference on computer vision*, pp. 3730–3738, 2015.
- [8] M. Mirza and S. Osindero, “Conditional generative adversarial nets,” *arXiv preprint arXiv:1411.1784*, 2014.
- [9] G. Antipov, M. Baccouche, and J.-L. Dugelay, “Face aging with conditional generative adversarial networks,” in *2017 IEEE International Conference on Image Processing (ICIP)*, pp. 2089–2093, IEEE, 2017.
- [10] G. Perarnau, J. Van De Weijer, B. Raducanu, and J. M. Álvarez, “Invertible conditional gans for image editing,” *arXiv preprint arXiv:1611.06355*, 2016.
- [11] A. Jaiswal, W. AbdAlmageed, Y. Wu, and P. Natarajan, “Bidirectional conditional generative adversarial networks,” in *Asian Conference on Computer Vision*, pp. 216–232, Springer, 2018.
- [12] Z. C. Lipton and S. Tripathi, “Precise recovery of latent vectors from generative adversarial networks,” *arXiv preprint arXiv:1702.04782*, 2017.
- [13] A. Creswell and A. A. Bharath, “Inverting the generator of a generative adversarial network,” *IEEE transactions on neural networks and learning systems*, 2018.
- [14] A. B. L. Larsen, S. K. Sønderby, H. Larochelle, and O. Winther, “Autoencoding beyond pixels using a learned similarity metric,” *arXiv preprint arXiv:1512.09300*, 2015.
- [15] J. Donahue, P. Krähenbühl, and T. Darrell, “Adversarial feature learning,” *arXiv preprint arXiv:1605.09782*, 2016.
- [16] V. Dumoulin, I. Belghazi, B. Poole, O. Mastropietro, A. Lamb, M. Arjovsky, and A. Courville, “Adversarially learned inference,” *arXiv preprint arXiv:1606.00704*, 2016.
- [17] J. Luo, Y. Xu, C. Tang, and J. Lv, “Learning inverse mapping by autoencoder based generative adversarial nets,” in *International Conference on Neural Information Processing*, pp. 207–216, Springer, 2017.
- [18] A. Heljakka, A. Solin, and J. Kannala, “Pioneer networks: Progressively growing generative autoencoder,” *arXiv preprint arXiv:1807.03026*, 2018.
- [19] D. Ulyanov, A. Vedaldi, and V. Lempitsky, “It takes (only) two: Adversarial generator-encoder networks,” in *Thirty-Second AAAI Conference on Artificial Intelligence*, 2018.
- [20] T. Karras, T. Aila, S. Laine, and J. Lehtinen, “Progressive growing of gans for improved quality, stability, and variation,” *arXiv preprint arXiv:1710.10196*, 2017.
- [21] M. Arjovsky, S. Chintala, and L. Bottou, “Wasserstein generative adversarial networks,” in *International Conference on Machine Learning*, pp. 214–223, 2017.
- [22] I. Gulrajani, F. Ahmed, M. Arjovsky, V. Dumoulin, and A. C. Courville, “Improved training of wasserstein gans,” in *Advances in Neural Information Processing Systems*, pp. 5767–5777, 2017.
- [23] N. Kodali, J. Abernethy, J. Hays, and Z. Kira, “On convergence and stability of gans,” *arXiv preprint arXiv:1705.07215*, 2017.
- [24] X. Mao, Q. Li, H. Xie, R. Y. Lau, Z. Wang, and S. Paul Smolley, “Least squares generative adversarial networks,” in *Proceedings of the IEEE International Conference on Computer Vision*, pp. 2794–2802, 2017.
- [25] D. Berthelot, T. Schumm, and L. Metz, “Began: Boundary equilibrium generative adversarial networks,” *arXiv preprint arXiv:1703.10717*, 2017.
- [26] T. Miyato, T. Kataoka, M. Koyama, and Y. Yoshida, “Spectral normalization for generative adversarial networks,” *arXiv preprint arXiv:1802.05957*, 2018.

- [27] T. Salimans, I. Goodfellow, W. Zaremba, V. Cheung, A. Radford, and X. Chen, “Improved techniques for training gans,” in *Advances in neural information processing systems*, pp. 2234–2242, 2016.
- [28] M. Lucic, K. Kurach, M. Michalski, S. Gelly, and O. Bousquet, “Are gans created equal? a large-scale study,” in *Advances in neural information processing systems*, pp. 700–709, 2018.
- [29] T. Karras, S. Laine, and T. Aila, “A style-based generator architecture for generative adversarial networks,” *arXiv preprint arXiv:1812.04948*, 2018.
- [30] X. Huang and S. Belongie, “Arbitrary style transfer in real-time with adaptive instance normalization,” in *Proceedings of the IEEE International Conference on Computer Vision*, pp. 1501–1510, 2017.
- [31] L. Deng, “The mnist database of handwritten digit images for machine learning research [best of the web],” *IEEE Signal Processing Magazine*, vol. 29, no. 6, pp. 141–142, 2012.
- [32] A. L. Maas, A. Y. Hannun, and A. Y. Ng, “Rectifier nonlinearities improve neural network acoustic models,” in *Proc. icml*, vol. 30, p. 3, 2013.
- [33] D. P. Kingma and J. Ba, “Adam: A method for stochastic optimization,” *arXiv preprint arXiv:1412.6980*, 2014.
- [34] S. Ioffe and C. Szegedy, “Batch normalization: Accelerating deep network training by reducing internal covariate shift,” *arXiv preprint arXiv:1502.03167*, 2015.
- [35] N. Srivastava, G. Hinton, A. Krizhevsky, I. Sutskever, and R. Salakhutdinov, “Dropout: a simple way to prevent neural networks from overfitting,” *The Journal of Machine Learning Research*, vol. 15, no. 1, pp. 1929–1958, 2014.
- [36] Y. Dogan and H. Yalim Keles, “Stability and diversity in generative adversarial networks,” in *2019 27th Signal Processing and Communications Applications Conference (SIU)*, IEEE, 2019.
- [37] H. Zhang, I. Goodfellow, D. Metaxas, and A. Odena, “Self-attention generative adversarial networks,” *arXiv preprint arXiv:1805.08318*, 2018.
- [38] M. Heusel, H. Ramsauer, T. Unterthiner, B. Nessler, and S. Hochreiter, “Gans trained by a two time-scale update rule converge to a local nash equilibrium,” in *Advances in Neural Information Processing Systems*, pp. 6626–6637, 2017.
- [39] M. D. Zeiler and R. Fergus, “Visualizing and understanding convolutional networks,” in *European conference on computer vision*, pp. 818–833, Springer, 2014.
- [40] K. Simonyan and A. Zisserman, “Very deep convolutional networks for large-scale image recognition,” *arXiv preprint arXiv:1409.1556*, 2014.
- [41] T. Tieleman and G. Hinton, “Lecture 6.5-rmsprop: Divide the gradient by a running average of its recent magnitude,” *COURSEERA: Neural networks for machine learning*, vol. 4, no. 2, pp. 26–31, 2012.
- [42] X.-m. Niu and Y.-h. Jiao, “An overview of perceptual hashing,” *Acta Electronica Sinica*, vol. 36, no. 7, pp. 1405–1411, 2008.
- [43] D. Petrov, “Wavelet image hash in Python.” <https://fullstackml.com/wavelet-image-hash-in-python-3504fdd282b5/>, 2016. [Online; accessed 19-June-2019].